

Europium diffusion in IG-110 nuclear graphite

T.M. Weilert^a, K.L. Walton^c, S.K. Loyalka^c, J.D. Brockman^{a,b,*}

^a Department of Chemistry, University of Missouri, 125 Chemistry Building, Columbia, MO 65211, United States

^b University of Missouri Research Reactor Center, University of Missouri, 1513 Research Park Dr. Columbia, MO 65211, United States

^c College of Engineering, University of Missouri, W1024 Lafferre Hall, Columbia, MO 65211, United States

*Corresponding Author E-mail Address: brockmanjd@missouri.edu (J.D. Brockman)

Abstract

Europium diffusion in graphite has been recognized to be of interest in high-temperature gas reactor safety analysis, particularly as an indicator of strontium diffusion. However, no measurements of europium diffusion coefficients have been reported in the literature. In this work, the effective diffusion coefficient of europium was measured using a time-release method. Natural europium was loaded into pre-milled unirradiated IG-110 graphite spheres using a pressurized acid digestion vessel. The time-release experiments were performed in the temperature range 1823 K – 1973 K using a SiC diffusion cell connected to an inductively-coupled plasma mass spectrometer (ICP-MS) via a He gas line. The results of this work are:

$$D_{Eu,IG-110} = \left(1.5 \times 10^{-3} \text{ m}^2/\text{s}\right) \exp\left(\frac{-2.87 \times 10^5 \text{ J/mol}}{RT}\right)$$

This effective diffusion coefficient can be used to aid in predictive modelling of europium transport in HTGRs.

1. Introduction

The high-temperature gas-cooled reactor (HTGR) uses a multi-layered fuel form consisting of a low-enriched uranium oxycarbide (UCO) or uranium oxide (UO₂) kernel surrounded by a buffer carbon layer, a dense inner pyrocarbon (PyC) layer, SiC, and a final outer layer of PyC. These multi-layered fuels, known as tristructural isotropic (TRISO) fuels, boast excellent fission product retention at operating temperatures between 700 °C – 950 °C [1, 2]. TRISO particles, once manufactured, are coated with a carbonaceous matrix material and then formed into either right cylindrical compacts or spheres, followed by heating to 800 °C – 1800 °C to cure the resin and reduce the impurity content [2]. Compacts are stacked within the structural graphite core of a prismatic reactor while the spheres make up the core of a pebble-bed reactor design. Flowing He is used to transfer the heat from the core, either directly to turbines or a steam generator.

Eu isotopes are low-yield, medium-lived fission products. ¹⁵⁴Eu and ¹⁵⁵Eu are often observed in post-irradiation analyses and heating tests and are sometimes used as an analog for ⁹⁰Sr release [3]. Several studies have examined Eu release from irradiated TRISO fuel particles and compacts with in-irradiation and post-irradiation investigations. Minato et al. [4] performed post-irradiation heating tests on irradiated UO₂ TRISO fuel particles sourced from deconsolidated fuel compacts. Despite there being no detected particle failures or observed Pd-induced decomposition of SiC, ¹⁵⁴Eu and ¹⁵⁵Eu were among several isotopes detected on the

surrounding structural graphite sink. These Eu fractional releases were as high as Cs in some cases [4].

Release of Eu from TRISO fuel was also observed in the Idaho National Laboratory's (INL) ongoing Advanced Gas Reactor Fuel Qualification and Development (AGR) Program. In AGR-1, UCO fuel kernels that were coated and compacted on a laboratory scale were irradiated at the Advanced Test Reactor (ATR) [5-13]. Post-irradiation examination (PIE) of AGR-1 capsules indicated release of Eu in excess of one TRISO particle equivalent [14-16]. This released Eu was retained in the surrounding matrix graphite and was only released during heating tests conducted between 1600 °C – 1800 °C [15-17]. PIE of the test train found ^{154}Eu in the metal capsule components, as well as the graphite fuel holders indicating Eu released further during the irradiation [14]. There were no detected TRISO failures throughout the course of the AGR-1 irradiation and the amount of Eu release exceeded the amount produced in a single TRISO particle, suggesting that Eu migrated through the SiC boundary during irradiation [14, 17].

In the AGR-2 test, some capsules were heated to higher average and peak temperatures compared to AGR-1 with Capsule 2 achieving a maximum time-average volume-average (TAVA) temperature of 1252 °C at the end of irradiation and a time-average peak temperature of 1360 °C. This was 163 °C higher than the maximum temperature of any capsule in the AGR-1 irradiation [17, 18]. The AGR-2 test utilized UCO and UO_2 kernels produced in an industrial scale coater and compacted on a laboratory scale at ORNL [19-32]. PIE of the AGR-2 test train showed Eu release through intact SiC with ^{154}Eu detected in the graphite fuel holder of Capsule 2 [3, 15, 33]. The level of ^{154}Eu outside of intact SiC layers in a compact from Capsule 2 exceeded what could be explained by observed coating failures [15]. Throughout all of Capsule 2, the total measured amount of ^{154}Eu was equivalent to 1410 particles' worth, or 3.7% of the capsule inventory [3].

The AGR-3/4 experiment was designed to measure fission product transport through compact matrix and structural graphite. This was achieved through the addition of 20 designed-to-fail (DTF) fuel particles in each of the 48 compacts (4 compacts per capsule) within the test train. [5, 34-36]. The fuel kernels of the DTF particles were identical to those of the driver particles and coated with only a thin layer of PyC [37, 38]. Capsule 7 was the highest temperature capsule in the AGR-3/4 irradiation with a TAVA temperature of 1345 °C and a time-averaged peak temperature of 1418 °C [39]. ^{154}Eu was detected in the inner matrix graphite ring of Capsule 7 in an amount equivalent to 229 particles, more than the 80 DTF particles originally present in the 4 compacts of the capsule [40, 41]. The AGR experiments demonstrate that Eu release is associated with increased temperature of the TRISO fuel and supports the possibility that Eu is capable of migrating through intact SiC [15]. Another potential source of Eu in structural graphite is from fission of U that is intrinsically present in the graphite [42].

Eu is well-retained in matrix graphite and it is not expected to migrate during normal reactor operation. Off-normal events such as a loss-of-forced coolant accident have the potential to raise the core temperature to 1620 °C [2]. These temperatures could enable enhanced Eu diffusion in the core. Structural and matrix graphite are both high-purity, fine-grain, high graphitization, high-isotropy graphites. Modern A3 matrix graphite is produced with different raw materials, manufactured using a hot-pressing method, and annealed at 1850 °C [43]. It has a average particle size of 11.3 μm [44], a bulk density of 1.3 – 1.7 g/cm^3 [43, 45, 46], and a total porosity of 20% [47]. IG-110 structural graphite is prepared using cold isostatic pressing with an annealing temperature at 2900 °C, has a grain size of 20 μm , and a density of 1.76 g/cm^3 . The total porosity of IG-110 graphite is 22.3% [48]. IG-110 graphite contains lower concentrations of

amorphous carbon and binder as well as a denser, more ordered pore structure. These properties offset each other as it relates to fission product diffusion and radionuclide transport in matrix and structural graphite has historically been treated as a collective process [49]. In previous experiments on Sr diffusion in A3 matrix graphite and structural graphite the reported activation energies ranged from 242 – 303 kJ/mol and 268 – 346 kJ/mol, respectively [50, 51]. This suggests that measurement of Eu diffusion in IG-110 allows for estimation of Eu diffusion in matrix graphite. The codes FRESCO and PARFUME could be used to track the migration of Eu in reactors. These codes utilize a single parameter to summarize the transport processes evaporation, adsorption, diffusion, and trapping into a single transport process known as the effective diffusion coefficient [50, 52].

There is little information on fission product diffusion in modern graphite grades and large experimental variation in experiments conducted on historical graphite. Several studies have attempted to measure Eu diffusion, but no diffusivity values have been provided. Cowan and Orth [53] examined diffusion rates of various fission products, including Eu, in irradiated slugs of graphite loaded with ^{235}U . They did not report noticeable diffusion of Eu except at 2400 °C after heating for 240 s. Orth [54] also examined trends in lanthanide and actinide diffusion in graphite at temperatures between 1600 °C – 2600 °C. While no diffusion constants were given, the author noted a strong correlation between diffusion rates and the boiling points of the elements under study. Hayashi et al. [55, 56] examined fission product distributions in OGL fuel assemblies taken from the Japan Materials Testing Reactor. The axial profiles of the block and graphite sleeve of the assembly were examined by means of high-purity germanium (HPGe) detection and the radial profiles were measured by lathe sectioning followed by HPGe detection of the graphite powder. Both ^{154}Eu and ^{155}Eu were detected, though only in the inner surface of the graphite sleeve. The Eu was theorized to be attributed solely to nuclear fission and not Eu impurity of the graphite [56]. Myers et al. [57] investigated the diffusion of Eu in a fuel test element of the Peach Bottom reactor. The source material contained precursors of the elements of interest which were then created through transmutation in the reactor. Radial profiles were created from the center post and crucible wall regions of these samples and while the authors stated they were able to fit the Eu profiles with the classical diffusion model no such fits were given. The successes and shortcomings of the above studies demonstrate a need for more quantitative exploration of Eu diffusion in graphite.

In this work, the effective diffusion of Eu was measured in IG-110 structural graphite using a time-release method. IG-110 is currently used in the primary core structures of the High Temperature Test Reactor in Japan and the HTR-10 and HTR-PM test reactors in China. Eu was loaded into pre-milled unirradiated IG-110 graphite spheres using a pressurized acid digestion vessel. The time-release experiments were performed in the temperature range 1823 K – 1973 K using a SiC diffusion cell connected to an inductively-coupled plasma mass spectrometer (ICP-MS) via a He gas line.

2. Theory

The time-release experiment described in this work has previously been successfully applied to effective diffusion measurements of Cs, I, Ag, and Sr in several types of graphite [51, 58-64]. The experiment assumes that migration and release of the Eu diffusant from the graphite

is dominated by diffusion, and that effects from adsorption and trapping are minimal [52]. The applicable diffusion equation in spherical coordinates is:

$$\frac{\partial C(r,t)}{\partial t} = \frac{1}{r^2} \frac{\partial}{\partial r} \left(D r^2 \frac{\partial C(r,t)}{\partial r} \right) \quad (1)$$

Together with the initial and boundary conditions:

$$C(r, 0) = C_0 \quad (2)$$

$$C(R, t) = 0 \quad (3)$$

Where D is the effective diffusion coefficient (m^2/s); $C(r, t) \geq 0$ is the concentration (g/m^3) of diffusant, in this case Eu, as a function of position and time; r is the radial coordinate (m); R is the radius of the sphere (m); t is the time (s); and C_0 is the known initial concentration (g/m^3) of diffusant. We also have that,

$$C(0, t) = \text{finite} \quad (4)$$

A uniform initial profile has been assumed for this work and subsequently Eqn. 1 has been solved via series expansion with the initial and boundary conditions described in Eqns. 2-4 to give the following cumulative fractional release equation:

$$F(t) = \frac{m_{\text{diffused}}(t)}{m_0} = 1 - \frac{6}{\pi^2} \sum_{n=1}^{\infty} \frac{1}{n^2} e^{-\left(\frac{n\pi}{R}\right)^2 D t} \quad (5)$$

Where $F(t)$ is the fractional release of diffusant at a given time, $m_{\text{diffused}}(t)$ (g) is the cumulative mass of Eu diffused at a given time, and m_0 (g) is the total mass of Eu initially present in the sample. For the purposes of this work, n was limited to 100 terms.

In time-release measurements of Ag diffusion, the authors compared results obtained from Eqn. 5, which assumes a uniform initial distribution of diffusant, to results obtained using the experimentally-determined concentration profile [63]. The difference in diffusivities obtained from the two assumptions were not statistically significant and therefore the authors have chosen to apply the same assumption of uniform distribution and use Eqn. 5 to fit the experimental data.

3. Experimental

Materials and Preparation

IG-110 structural graphite was milled to spheres with diameters of ~ 0.32 cm. The pre-milled spheres were placed in the 45 mL polytetrafluoroethylene (PTFE) sleeve of a Parr Model 4744 pressurized acid digestion vessel to which was added 15 mL of a 1000 part-per-million (ppm) $\text{Eu}(\text{NO}_3)_2$ standard (Inorganic Ventures, 7% (v/v) HNO_3) and 5 mL of high-purity water. The parr bomb was assembled and then heated for four alternating cycles of 508 K for 2 hours and 373 K for 1 hour. After cooling, the vessel was disassembled, and the spheres were removed and placed in a vacuum oven at ~ 373 K where they remained overnight. The next day they were heated to 773 K for 30 minutes to dissociate remaining nitrates. The spheres were then individually sanded with Al_2O_3 sandpaper, sonicated in high-purity water to remove dust, and

then dried on a hot plate. The final diameter of each sphere was measured with calipers to the nearest 0.025 mm. This method produced IG-110 spheres with an average mass of 1.64 μg Eu and average diameter of 0.312 ± 0.003 cm.

The above-stated average mass of Eu in the samples was measured using standard comparator instrumented neutron activation analysis (INAA). Standards containing ~ 3 μg each of Eu were prepared by drying aliquots of a 1000 ppm standard on filter paper. The samples, once prepared, were irradiated with the standards in the University of Missouri Research Reactor for 5-10 seconds at a thermal neutron flux of 5.5×10^{13} n/cm²/s. The samples and standards were then counted for 20 minutes each on a high-purity germanium (HPGe) detector; the 842 keV decay line was used for quantification.

A sample was selected from the batch for radial distribution measurements. The sample was bisected with a stainless-steel razor blade and the flat faces were smoothed with Al₂O₃ sandpaper. One of the flat faces was then set facing a Photon Machines 192 nm laser which was connected to a NexION[®] 300x ICP-MS. The laser operated with a power density of 2 mJ/cm² and 10 Hz pulse frequency. The laser produced 40 μm spot sizes and samplings were taken every 100 μm across the diameter of the sample. The sampling direction was rotated 45° clockwise after every completed line; this was repeated four times and the results were averaged. This procedure was used on a random sample selected from the initial loading batch and was repeated on the sample which was used to measure the Eu diffusion coefficient at 1873 K.

Diffusion Measurements

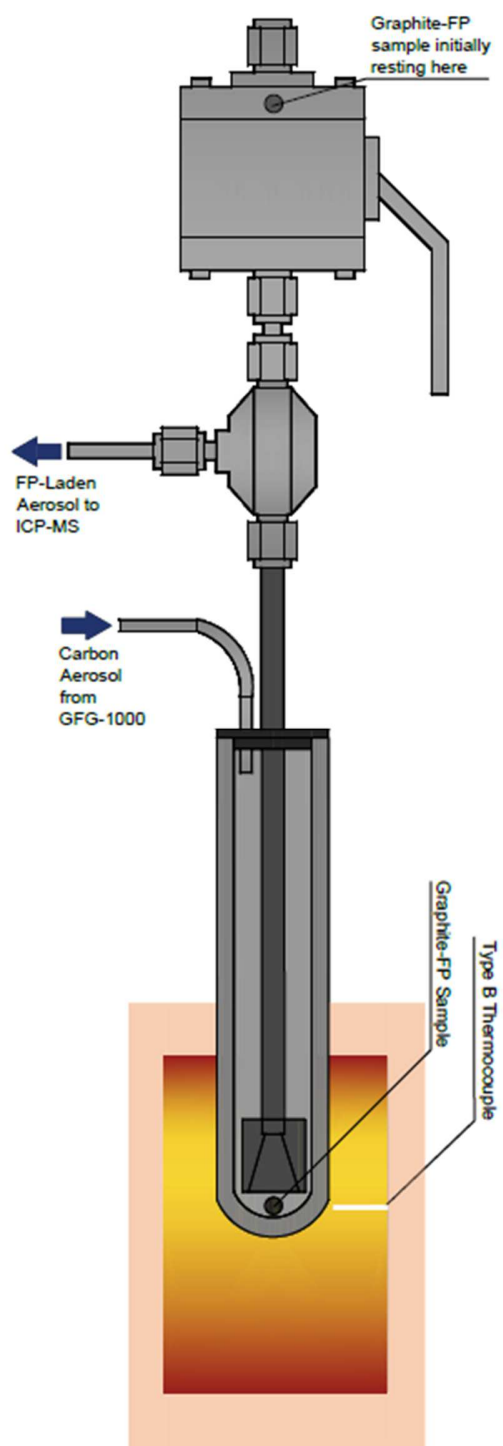


Figure 1: The SiC time-release diffusion cell. “FP” refers to fission product however the Eu used was from a natural source [51].

The time-release method used here has been described in previous publications and is only briefly described here [51, 58-64]. In Fig. 1, a Eu-loaded graphite sample was left in the top of a ball valve set on top of a Saint Gobain Hexaloy® SiC diffusion cell. The cell was set in a

Model ST-1700C SentroTech box furnace with a maximum temperature capability of 1700 °C. While the furnace heated to the experimental temperature, ultra-high purity He flowed through the cell to displace room air. The ball valve was left in a partially open position to allow He to flow into the sample chamber without letting the sample fall through. The He was first directed through a Palas GFG-1000 carbon aerosol generator, modified for use with He. The operating specifics of this generator have been described in Carter, et al. [58]. The generator produced carbon nanoparticles entrained in He flowing at 2 L/min. The He flow was reduced to 1 L/min prior to entering the SiC chamber using a splitter valve. After the furnace had reached the experimental temperature the ICP-MS was started and optimized. Background Eu measurements were taken for approximately 1 hour, after which the ball valve was opened, allowing the sample to drop into the preheated diffusion cell. Released Eu was carried to the ICP-MS via the He-carbon aerosol and injected through a dual-inlet spray chamber. The second inlet was used to introduce a 1 ng/g In internal standard which allowed for correction of instrumental drift. Temperature monitoring was achieved through a Pt/Rh thermocouple installed in the furnace and placed at the base of the diffusion cell, see Fig. 1. These time-release measurements were conducted in the temperature range 1823 K – 1973 K in 50 K intervals. A COMSOL multi-physics model, described in Appendix A, was used to demonstrate a negligible temperature distribution near the sample location.

Data Analysis

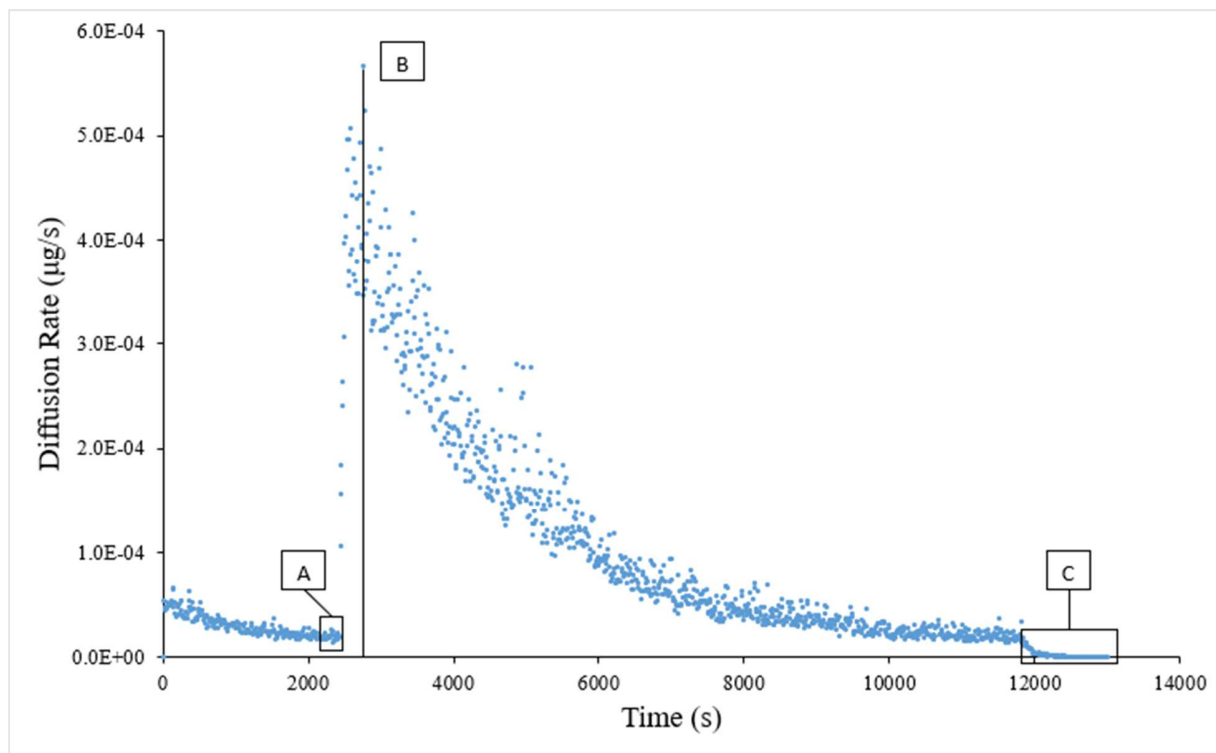


Figure 2: Europium time-release experiment at 1873 K. [A] is the baseline just before the sample was dropped into the diffusion cell. [B] is the peak rate of diffusion after sample introduction. [C] is the signal recorded after the furnace had been shut down.

Once experiments were complete, INAA was performed on the samples in the same manner as previously described in order to determine the total mass loss of Eu over the course of each experiment. This mass loss was used to convert the mass spectrometer signal of counts/second to units of mass loss/second. A background correction was applied to each experiment in one of two ways: by calculating a constant background based on an average of the last ten measurements before sample introduction (feature A in Fig. 2) and subtracting that value from all subsequent measurements, or by fitting the background to a best-fit exponential equation and subtracting the values derived from that equation from the remainder of the measurements. In general, the first method was favored due to its greater simplicity. However, in some cases the sample was introduced into the chamber before the background had adequately decayed. The difference in the calculated diffusivities when comparing these two methods was an average of 4%.

After the sample was introduced, the Eu signal rapidly increased until it reached a peak, shown as feature B in Fig. 2. After several hours, when the release signal had decayed nearly to baseline (indicating a majority of the Eu had been released), the furnace was stopped and ICP-MS measurements continued for 20 minutes as the temperature decreased. This is shown as feature C in Fig. 2. The counts in this region make up less than 1% of the total counts for the experiment and therefore this decay period is not corrected for. The signal acquired before the peak was not used in the cumulative release fit as it was attributed to release of Eu from the graphite surface and nondiffusion-dominated processes. The signal before the peak was summed, converted to mass loss, and subtracted from the initial mass of Eu present in the sample. The remainder of the curve was converted to instantaneous fractional release by multiplying by a calibration factor, $F_{calibration}$ (g/count), which was equal to the corrected mass loss divided by the total background-corrected counts in the diffusion region. The calibration factor was then multiplied by the count rate (counts/s) at each time point to calculate the release rate (g/s). Finally, the total fractional release was calculated at each time point by integration of the release rate over the region of interest to calculate the mass diffused and dividing by the initial mass of Eu present in the sample, as described in Carter et al. [58]. The experimental fractional release was then fit to Eqn. 5, as previously described. All of the above steps occurred after normalizing to the signal of the In standard.

The Arrhenius equation was used to demonstrate the temperature dependence of the Eu diffusion coefficient, Eqn. 6:

$$D = D_0 e^{-E_a/RT} \quad (6)$$

Where D_0 is the pre-exponential factor (m^2/s) and E_a is the activation energy (kJ/mol). Uncertainties in the pre-exponential factor and activation energy were calculated from standard errors of the best fit linear regression.

4. Results

Figure 3 presents the results of the radial distribution measurements of Eu after the pressure vessel loading. The slope of the average distribution was 17,534 counts/cm, 95% CI [-24,104 59,173]. An F-test revealed there was no significant relationship between the radial distance and the Eu distribution ($F_{1,13} = 0.84$, $p = 0.38$). A flat diffusant profile was assumed, and Eqn. 5 was used to calculate the effective diffusion coefficients. Previous work with Ag has

indicated no significant difference between effective diffusivities calculated using the measured profile vs. a flat profile [64].

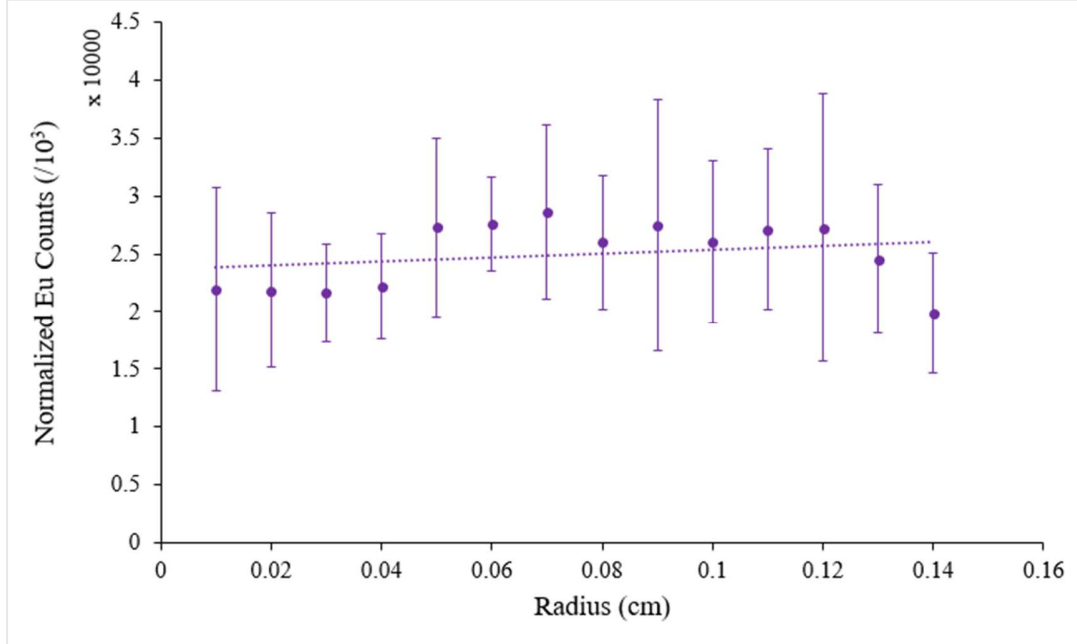


Figure 3: Radial distribution of Eu in an IG-110 sphere loaded using a pressure vessel.

Diffusion measurements were performed at four temperatures, beginning with 1823 K. Table 1 presents the test temperature, initial and final Eu mass, and the effective diffusivity of Eu, the variance, the mean absolute value of the error, and the exposure time for each experiment performed. The variance, thus standard error, was calculated from the Hessian matrix of the least squares fit using Excel [65]. The mean absolute value of the error (MAE) is reported as a goodness of fit between the simulated and the measured cumulative release using Eqn. 7.

$$error = \left| \frac{y - y_{fit}}{y} \right| \quad (7)$$

Where y_{fit} is the predicted cumulative release fraction and y is the measured cumulative release fraction. These results are shown again in Fig. 4 in the form of the experimentally derived fractional release curves with the best-fit solutions to Eqn. 5 super-imposed on the accompanying curve.

Table 1: The experimental temperature, initial and final Eu mass, calculated diffusion coefficient, MAE, and exposure time for each experiment.

Test Temperature (K)	Initial Eu Mass (μg)	Final Eu Mass (μg)	Diffusion Coefficient (m^2/s)	MAE	Exposure Time (s)
1823	1.40	0.62	$8.87 (1.8) \times 10^{-12}$	10.5%	9390
1873	1.69	0.42	$1.51 (0.20) \times 10^{-11}$	17.0%	14190
1923	1.86	0.45	$2.74 (0.47) \times 10^{-11}$	14.2%	8190
1973	1.62	0.36	$3.58 (0.75) \times 10^{-11}$	22.5%	5790

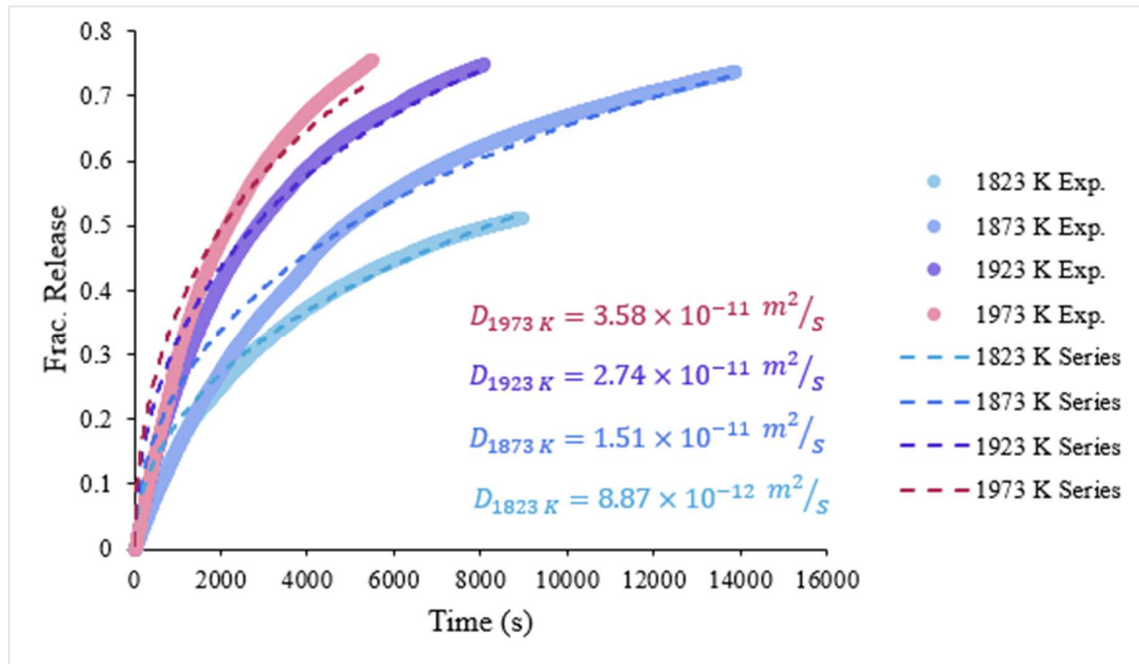


Figure 4: Experimental fractional release curves of Eu in IG-110 graphite taken between 1823 K and 1973 K and the best-fit solutions to Eqn. 5.

The Arrhenius parameters, shown in Table 2, were derived by fitting the Arrhenius diffusion coefficient to the reciprocal temperature using a weighted linear least squares approach. The results were linear over the experimental temperature range. The accompanying Arrhenius plot is presented in Fig. 5 along with results of earlier measurements for Sr diffusion over a similar temperature range using the same time-release method [51].

Table 2: Calculated Arrhenius parameters of Eu diffusion in IG-110 graphite between 1823 K – 1973 K.

Diffusant	D_0 (m^2/s)	$\pm \Delta D_0$ (m^2/s)	E_a (kJ/mol)	$\pm \Delta E_a$ (kJ/mol)
Eu	1.5×10^{-3}	3.8×10^{-4}	287	26

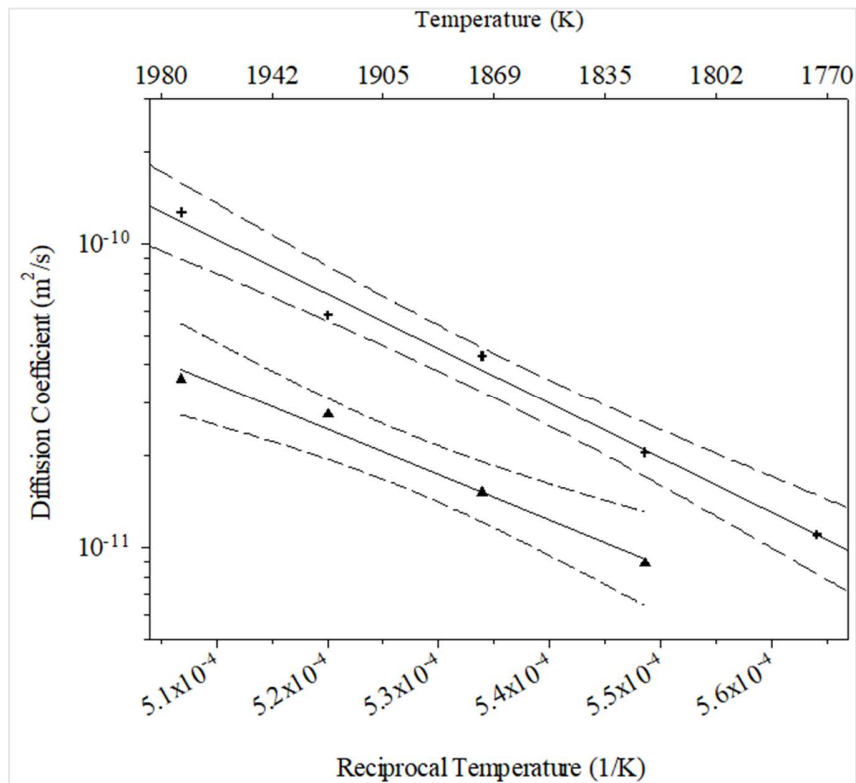


Figure 5: Arrhenius plot of Sr and Eu diffusion in unirradiated IG-110 graphite [51]. The Sr plot is the upper curve and the Eu plot is shown below. The dashed lines represent the respective 95% confidence intervals.

5. Discussion

The time-release method described in this work has previously been successfully applied to diffusion measurements of Cs, I, Ag, and most recently Sr in several types of nuclear graphite [51, 58-63]. The Arrhenius parameters of Sr were $E_a = 346 (\pm 22)$ kJ/mol and $D_0 = 1.7 (\pm 1.3) \times 10^{-11}$ m²/s over the temperature range 1773 K – 1973 K [51]. The individual Sr diffusion measurements had resulting diffusivities approximately 3 times greater than the temperature-equivalent Eu measurements. The slope of the best-fit line for Sr was such that it would intersect the Eu best-fit line at 1516 K, below which Eu would exhibit greater diffusivities. This is in keeping with observations obtained from AGR experiments, discussed earlier, in which Eu and Sr were known to exhibit similar diffusive behaviors with Eu release in general greater than that of Sr [3].

Concentration dependencies of diffusion are an important consideration in diffusivity studies. One advantage of the time-release method used in this work over the depth profiling method is that experiments can be conducted at low diffusant concentrations. The high energy binding sites dominate diffusion processes at low diffusant concentrations. As the concentration of diffusant increases, weaker binding sites begin to contribute to diffusion processes resulting in increased rates of migration [66]. Cs and Sr are known to exhibit relevant changes in diffusion rates when the concentration of the element under study increases above a certain point [66-68]. For example, the “limit” of concentration for Sr in graphite, under which diffusion is believed to not be affected by concentration, is 62 μ g Sr/g graphite [68]. Eu is expected to exhibit a similar

concentration dependency above a threshold concentration value, however, to the best of the authors' knowledge, the value of the threshold is unknown. The graphite samples used in this study had an average radius of 0.156 cm and an average Eu loading content of 1.64 μg . Considering the stated density of IG-110 of 1.76 g/cm^3 , this equates to an average concentration of 59 μg Eu/g graphite. This amount is close to the accepted limit for Sr but a direct comparison cannot be made. Further investigations into a possible Eu concentration dependency should be made in future studies.

Similar to the Sr diffusion studies [51], the Eu experimental fractional releases did not initially align well with the best-fit solutions to Eqn. 5. In the four fractional release plots shown in Fig. 4, Eqn. 5 overpredicts the release rate in the first 1000 s – 4000 s of the experiments, after which the series solution was in good agreement with the experimental releases. In diffusion studies it is common to ignore effects related to sorption or trapping; these are factored into the effective diffusion coefficient, but their contributions are considered minimal [52]. Despite that, the overprediction of Eqn. 5 in the first few thousand seconds of each experiment could be the result of sorption at the surface of the sphere competing with diffusion as the rate limiting step or, alternatively, some transport effects (e.g., free flight of molecules) other than diffusion playing a role. In the Eu distribution, see Fig. 3, Eu was measured at the surface of the sphere which is a violation of the initial condition reported in Eqn. 3. This violation could have led to deviation of Eqn. 5, particularly early in the experiments. To test the impact of the poor early time fits, diffusion coefficients were calculated wherein the first 10%, 20%, 30%, and 40% of the total fractional release was ignored and Eqn. 5 was only fit to the remainder of the curve. For all four time-release experiments over all four tested conditions the change in the effective diffusion coefficient was no more than 8%. This is well within the uncertainties reported in Table 1 and indicates that the reported effective diffusivities are a good representation of the experimental fractional release curves.

The chemical form of diffusant could also have a significant effect on its rate of diffusion. The heating step to 773 K, described in Section 3, was intended to dissociate $\text{Eu}(\text{NO}_3)_3$. This dissociation likely led to the Eu being in the chemical form of either Eu_2O_3 or EuO . Thermodynamic calculations on the suitability of binary oxides for epitaxy source materials reported that at low partial pressures of O_2 , the dominant form of Eu over the two Eu oxides was Eu metal at temperatures above 1800 K [69]. Near 1800 K the calculated partial pressure of EuO and Eu metal were similar, and both could thermodynamically be present in the graphite sphere. In the high-purity He environment of the diffusion cell the O_2 partial pressure would be very low and would promote the decomposition of the Eu oxide to Eu metal. The presence of both EuO and Eu at the beginning of the experiments could account for the overprediction of the experimental data early in the release profile.

The temperature of the furnace was measured using a thermocouple located 2.5 cm from the sample position inside the SiC chamber. It is possible that the temperature inside of the SiC tube housing the test sample was cooled by the flow of He entering the chamber. A COMSOL multi-physics model, described in Appendix A, was used to determine the temperature distribution near the sample location. The model indicates a temperature drop of 40 – 48 K over the experimental temperature range of 1823 K – 1973 K. The model does not account for the heat exchange between the tube assembly and the insulation or the fact that the thermocouple regulating the oven temperature is 2.5 cm from the sample location. The model predicts a sample temperature of 1783 K at the experimental temperature of 1823 K, which is 21 K lower than the boiling point of Eu. This suggests that the COMSOL model overpredicts the temperature drop at

the sample location. Calculating the Arrhenius parameters using the COMSOL model temperatures instead of the experimental temperatures results in a activation energy of 288 ± 26 kJ/mol and a pre-exponential factor of 2.48 ± 0.71 m²/s. The activation energy is unchanged, while the pre-exponential factor is different than the values reported in Table 2.

The IG-110 graphite used in this study is manufactured using a cold isostatic molding method and is a fine-grained, petroleum coke-based nuclear graphite with a porosity volume of 22.3% [48]. Variations in these stated properties (e.g. molding method, grain size, coke source, and porosity) will affect both base diffusion rates and microstructural changes resulting from oxidation and neutron irradiation which will in turn also affect fission product diffusion. IG-110 was chosen due to its prevalence in currently operating HTGRs and the work presented here has established a baseline of information on Eu diffusion in structural graphite and initiated an approximation of Eu diffusion in fuel component graphite materials. While IG-110 graphite is not the representative of diffusion in matrix and PyC, analysis of diffusion in structural graphite provides an approximation of diffusion behavior in fuel component graphite materials and accurate insight into diffusion of Eu in structural graphite components. Much work is still needed on comparative studies with alternative grades of structural graphite as well as matrix graphites to assess the validity of the current standard of treating fission product diffusion in these differing materials as a collective process [49].

6. Conclusions and Future Work

The diffusion of Eu in graphite has often been overlooked. As a result, little is known about its rates of diffusion, what influence other fission products may have in slowing or increasing those diffusion rates, as well as various effects related to structural damage of the graphite and concentration dependencies. In this work, Eu diffusion in IG-110 structural graphite was measured using a time-release method with resulting Arrhenius parameters of $E_a = 287$ (26) kJ/mol and $D_0 = 1.5$ (0.38) $\times 10^{-3}$ m²/s. This has provided accurate information on the diffusion of Eu in structural graphite and an approximation of Eu diffusion in graphitic matrices.

7. Acknowledgments

This research has been supported by the U.S. Department of Energy Nuclear Energy University Program grant NEUP-12830, and an Integrated University Program Fellowship grant (DE-NE000118 Mod 007) towards support of T.M. Weilert.

Appendix: Computation of Heat Transfer in the Diffusion cell

A simple model for multi-physics simulation was used to determine any cooling effects from the flowing helium gas into the diffusion cell assembly. A conjugate heat transfer model with radiative heat transfer was implemented in COMSOL Multiphysics using Heat Transfer in Solids and Fluids, Laminar Flow, and Surface to Surface Radiation physics modules. Figure A.1 shows the SiC diffusion cell assembly and a representation of the furnace chamber. Information on the size and position of the heating elements could not be obtained for the simulation. Tables A.1 and A.2 provide the selected physics on the domains and boundaries, respectively, for each COMSOL physics module. Material data commonly available to the COMSOL program were used. Thus, AISI 4340 was chosen for the endcap instead of setting up data for stainless steel.

The model assumes the inserted portion of the diffusion cell assembly is heated in an air enclosure with fixed temperature walls. The size of the chamber is 0.2 m×0.2 m×0.2 m. The diffusion cell assembly portion outside the chamber was allowed to cool with natural convection and radiant energy. For natural convection, the heat transfer coefficient was 5 W/(m² K¹). The helium flow from the spark generator was split between the diffusion cell assembly and HEPA filter, such that helium flow into the diffusion cell is 1 L/min. The Reynolds number at the inlet was estimated to be about 50, where the gas is at ambient temperature (293 K), and the kinematic viscosity is at its lowest. The Reynolds number will decrease throughout the diffusion cell, ensuring laminar flow. At the current gas density, no slip was assumed at the Wall boundary conditions for the Laminar flow. All fluid walls were also gray diffusive surfaces for the Surface to Surface radiation, as seen in Table A.2. Chamber wall emissivity was chosen to be 0.8. The remaining material properties were from COMSOL's material library.

The temperature distribution around the graphite sphere would be due to the furnace design and heat losses through the port at the top of the furnace for the diffusion cell assembly. The magnitude of the linear flow velocity is given in Fig. A.2. The helium flow is relatively slow in the annular region of the assembly compared to the flow exiting through the inner SiC tube. The valve at the top of the diffusion cell assembly would create a higher resistance to the flow than in the model. The temperature distribution is given in Figs. A.3 and A.4. The model shows that the sphere is approximately 48 K lower than the chamber walls at 1973 K. However, the model does not account for the heat exchange between the SiC tube assembly and the insulation or the fact that the thermocouple that regulates the oven temperature is 2.5 cm from the sample location in the center of the furnace chamber. The model shows the temperature of the sphere to be 40 K lower than the chamber walls at 1823 K, which is 21 degrees below the boiling point of Eu metal. With the model assumptions, no cooling occurs until outside of the chamber. While fixed wall temperatures are not realistic, the ST-1700-888 is heavily insulated at the walls and door. The model confirms that the sample temperature is not significantly cooled during the experiment.

Table A.1: Domain materials and physics for COMSOL model.

Domain	Material	Physics		
		Heat Transfer in Solids and Fluids	Laminar Flow	Surface to Surface Radiation
SiC Tubes and Nozzle	Silicon Carbide	Solid	N/A	Opaque
Endcap	Steel AISI 4340	Solid	N/A	Opaque
Graphite Sphere	Graphite	Solid	N/A	Opaque
Helium	Helium	Fluid	Fluid	Transparent
Air	Air	Fluid	Fluid	Transparent

Table A.2: Boundary conditions for various surfaces for each physics module used in the model.

Boundary	Physics		
	Heat Transfer in Solids and Fluids	Laminar Flow	Surface-to-Surface Radiation
Endcap			
Exterior	Surface-Ambient Radiation Heat Flux	N/A	N/A
Bottom	N/A	Wall (No Slip)	Diffusive Surface
Outer Tube Exposed			
Exterior	Surface-Ambient Radiation Heat Flux	N/A	N/A
Interior	N/A	Wall (No Slip)	Diffusive Surface
Outer Tube Heated Zone	N/A	Wall (No Slip)	Diffusive Surface
Inner Tube/Nozzle	N/A	Wall (No Slip)	Diffusive Surface
Chamber Walls	Temperature	Wall (No Slip)	Diffusive Surface
Graphite Sphere	NA	Wall (No Slip)	Diffusive Surface
Helium			
Inlet	Inflow	Inlet	N/A
Outlet	Outflow	Outlet	N/A

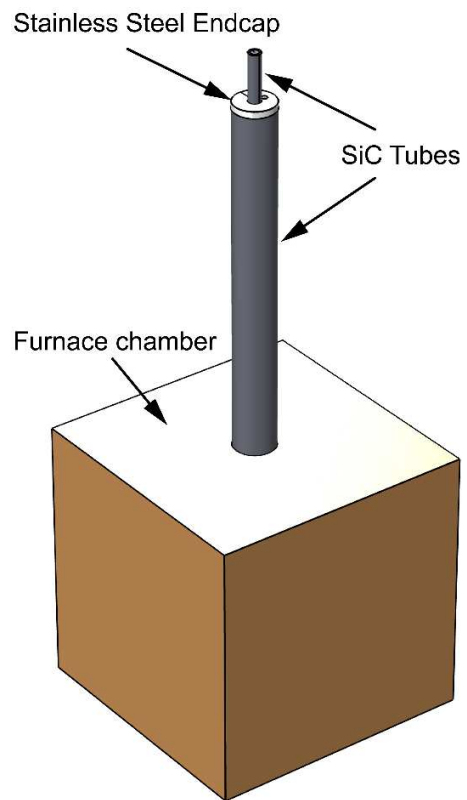


Figure A.1: Rendered geometry used for conjugate heat transfer with radiant heat transfer in COMSOL.

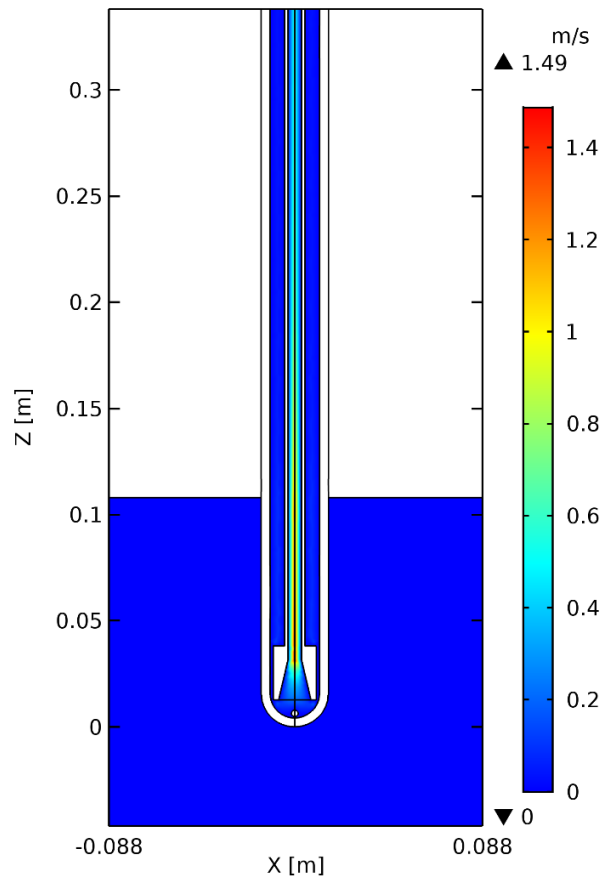


Figure A.2: Magnitude linear velocity of helium in the SiC diffusion in the XZ-plane at y=0.

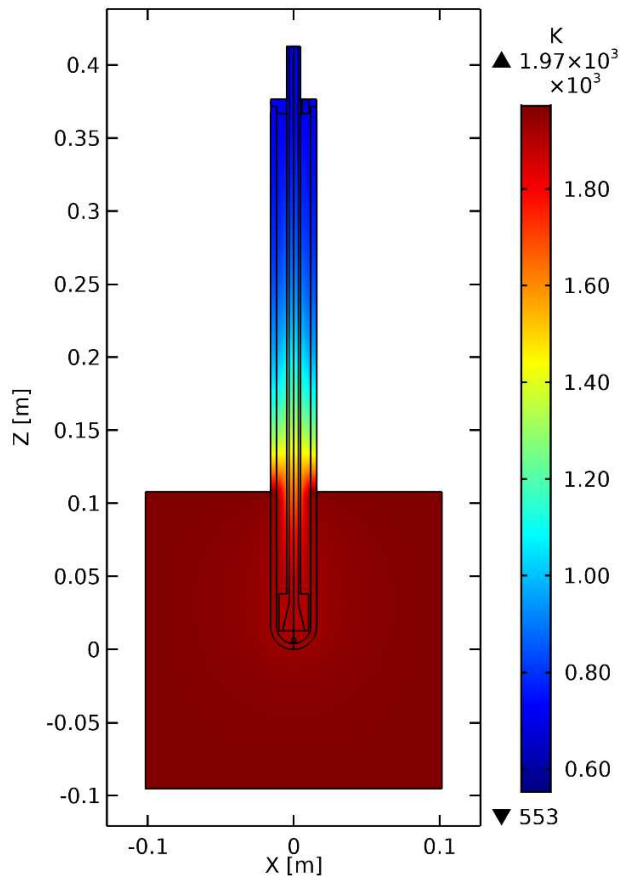


Figure A.3: Temperature distribution in the XZ-plane at y=0.

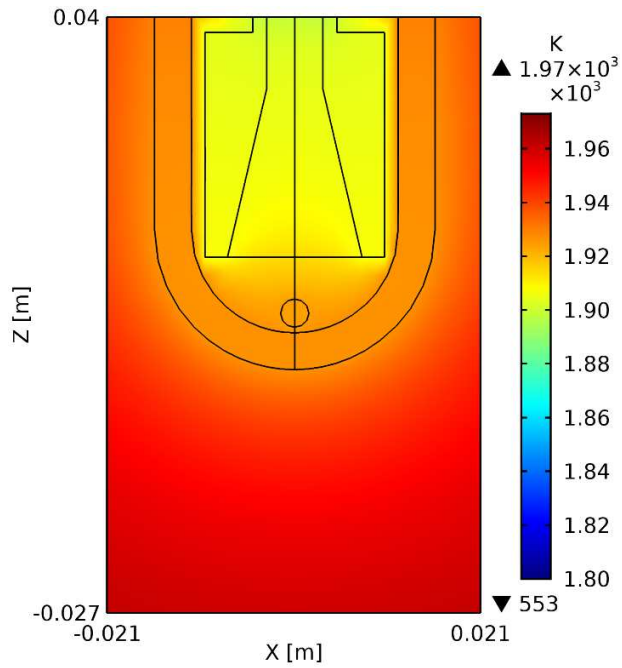


Figure A.4: Temperature distribution in the XZ-plane at y=0.

References

- [1] K. Verfondern, H. Nabielek, J.M. Kendall, Coated particle fuel for high temperature gas cooled reactors, *Nucl. Eng. Technol.* 39(5) (2007) 603-616, <https://doi.org/10.5516/NET.2007.39.5.603>.
- [2] High Temperature Gas Cooled Reactor Fuels and Materials, International Atomic Energy Agency, Vienna, Austria, 2010, p. 182.
- [3] J.D. Stempien, P.A. Demkowicz, AGR-2 Irradiation Experiment Fission Product Mass Balance, Idaho National Laboratory, Idaho Falls, ID, 2019.
- [4] K. Minato, T. Ogawa, K. Fukuda, H. Sekino, H. Miyanishi, S. Kado, I. Takahashi, Release behavior of metallic fission products from HTGR fuel particles at 1600 to 1900°C, *J. Nucl. Mater.* 202(1-2) (1993) 47-53, [https://doi.org/10.1016/0022-3115\(93\)90027-V](https://doi.org/10.1016/0022-3115(93)90027-V).
- [5] C.M. Barnes, AGR-1 Fuel Product Specification and Characterization Guidance, Idaho National Laboratory, Idaho Falls, ID, 2006a, p. 46.
- [6] J.D. Hunn, R.A. Lowden, Data Compilation for AGR-1 Baseline Coated Particle Composite LEU01-46T, Oak Ridge National Laboratory, Oak Ridge, TN, 2006a, p. 235.
- [7] J.D. Hunn, R.A. Lowden, Data Compilation for AGR-1 Variant 1 Coated Particle Composite LEU01-47T, Oak Ridge National Laboratory, Oak Ridge, TN, 2006b, p. 192.
- [8] J.D. Hunn, R.A. Lowden, Data Compilation for AGR-1 Variant 2 Coated Particle Composite LEU01-48T, Oak Ridge National Laboratory, Oak Ridge, TN, 2006c, p. 162.
- [9] J.D. Hunn, R.A. Lowden, Data Compilation for AGR-1 Variant 3 Coated Particle Composite LEU01-49T, Oak Ridge National Laboratory, Oak Ridge, TN, 2006d, p. 186.
- [10] J.D. Hunn, F.C. Montgomery, P.J. Pappano, Data Compilation for AGR-1 Baseline Compact Lot LEU01-46T-Z, Oak Ridge National Laboratory, Oak Ridge, TN, 2006a, p. 51.
- [11] J.D. Hunn, F.C. Montgomery, P.J. Pappano, Data Compilation for AGR-1 Variant 1 Compact Lot LEU01-47T-Z, Oak Ridge National Laboratory, Oak Ridge, TN, 2006b, p. 53.
- [12] J.D. Hunn, F.C. Montgomery, P.J. Pappano, Data Compilation for AGR-1 Variant 2 Compact Lot LEU01-48T-Z, Oak Ridge National Laboratory, Oak Ridge, TN, 2006c, p. 43.
- [13] J.D. Hunn, F.C. Montgomery, P.J. Pappano, Data Compilation for AGR-1 Variant 3 Compact Lot LEU01-49T-Z, Oak Ridge National Laboratory, Oak Ridge, TN, 2006d, p. 44.
- [14] P.A. Demkowicz, J.M. Harp, P.L. Winston, S.A. Ploger, Analysis of Fission Products on the AGR-1 Capsule Components, Idaho National Laboratory, Idaho Falls, ID, 2013, p. 50.
- [15] J.D. Hunn, C.A. Baldwin, F.C. Montgomery, T.J. Gerczak, R.N. Morris, G.W. Helmreich, P.A. Demkowicz, J.M. Harp, J.D. Stempien, Initial examination of fuel compacts and TRISO particles from the US AGR-2 irradiation test, *Nucl. Eng. Des.* 329 (2018) 89-101, <http://dx.doi.org/10.1016/j.nucengdes.2017.09.017>.
- [16] P.A. Demkowicz, E.L. Reber, D.M. Scates, L. Scott, B.P. Collin, First high temperature safety tests of AGR-1 TRISO fuel with the Fuel Accident Condition Simulator (FACS) Furnace, *J. Nucl. Mater.* 464 (2015) 320-330, <http://dx.doi.org/10.1016/j.jnucmat.2015.05.006>.
- [17] P.A. Demkowicz, J.D. Hunn, R.N. Morris, I. van Rooyen, T. Gerczak, J.M. Harp, S.A. Ploger, AGR-1 Post Irradiation Examination Final Report, Idaho National Laboratory, Idaho Falls, ID, 2015, p. 132.
- [18] B.P. Collin, AGR-2 Irradiation Test Final As-Run Report, Idaho National Laboratory, Idaho Falls, ID, 2014, p. 87.
- [19] C.M. Barnes, AGR-2 Fuel Specification, Idaho National Laboratory, Idaho Falls, ID, 2009.

- [20] BWXT, Industrial Fuel Fabrication and Development Lot G73AA-10-69308, Data Certification Package, 2008.
- [21] BWXT, Industrial Fuel Fabrication and Development Lot G73I-14-69307, Data Certification Package, 2008.
- [22] BWXT, Industrial Fuel Fabrication and Development Lot G73J-14-93071A, G73J-14-93073A, G73J-14-93074A, Data Certification Package, 2008.
- [23] BWXT, Industrial Fuel Fabrication and Development Lot G73H-10-93085B, Data Certification Package, 2009.
- [24] J.D. Hunn, Data Compilation for AGR-2 Baseline Coated Particle Batch G73J-14-93071A, Oak Ridge National Laboratory, Oak Ridge, TN, 2008, p. 15.
- [25] J.D. Hunn, Data Compilation for AGR-2 Baseline Coated Particle Batch G73J-14-93072A, Oak Ridge National Laboratory, Oak Ridge, TN, 2008, p. 13.
- [26] J.D. Hunn, Data Compilation for AGR-2 UCO Variant Coated Particle Batch G73J-14-93073A, Oak Ridge National Laboratory, Oak Ridge, TN, 2008, p. 12.
- [27] J.D. Hunn, Data Compilation for AGR-2 UCO Variant Coated Particle Batch G73J-14-93074A, Oak Ridge National Laboratory, Oak Ridge, TN, 2008, p. 12.
- [28] J.D. Hunn, Data Compilation for AGR-2 B&W UO₂ Coated Particle Batch G73H-10-93085B, Oak Ridge National Laboratory, Oak Ridge, TN, 2010, p. 18.
- [29] J.D. Hunn, F.C. Montgomery, P.J. Pappano, Data Compilation for AGR-2 UCO Baseline Compact Lot LEU07-OP1-Z, Oak Ridge National Laboratory, Oak Ridge, TN, 2009, p. 130.
- [30] J.D. Hunn, F.C. Montgomery, P.J. Pappano, Data Compilation for AGR-2 UCO Variant Compact Lot LEU06-OP1-Z, Oak Ridge National Laboratory, Oak Ridge, TN, 2009, p. 114.
- [31] J.D. Hunn, F.C. Montgomery, P.J. Pappano, Data Compilation for AGR-2 UCO Baseline Compact Lot LEU09-OP2-Z, Oak Ridge National Laboratory, Oak Ridge, TN, 2010, p. 132.
- [32] J.D. Hunn, F.C. Montgomery, P.J. Pappano, Data Compilation for AGR-2 B&W UO₂ Compact Lot LEU11-OP2-Z, Oak Ridge National Laboratory, Oak Ridge, TN, 2010, p. 165.
- [33] J.M. Harp, P.A. Demkowicz, J.D. Stempien, Fission Product Inventory and Burnup Evaluation of the AGR-2 Irradiation by Gamma Spectrometry, 2016 International Topical Meeting on High Temperature Reactor Technology (HTR 2016), Las Vegas, NV, 2016, p. 11.
- [34] BWXT, Industrial Fuel Fabrication and Development Lot G73V-20-69303, Data Certification Package, 2006.
- [35] A.K. Kercher, B.C. Jolly, F.C. Montgomery, C. Silva, J.D. Hunn, Data Compilation for AGR-3/4 Designed-To-Fail (DTF) Fuel Particle Batch LEU03-07DTF, Oak Ridge National Laboratory, Oak Ridge, TN, 2011, p. 70.
- [36] J.D. Hunn, R.A. Lowden, Data Compilation for AGR-3/4 Driver Fuel Coated Particle Composite LEU03-09T, Oak Ridge National Laboratory, Oak Ridge, TN, 2007, p. 187.
- [37] C.M. Barnes, AGR-3 & 4 Fuel Product Specification, Idaho National Laboratory, Idaho Falls, ID, 2006b.
- [38] D.W. Marshall, AGR-3/4 DTF Fuel and Capsule Component Material Specifications, 2011.
- [39] B.P. Collin, P.A. Demkowicz, D.A. Petti, G.L. Hawkes, J. Palmer, B.T. Pham, D.M. Scates, J.W. Sterbentz, The AGR-3/4 fission product transport irradiation experiment, Nucl. Eng. Des. 327 (2018) 212-227, <https://doi.org/10.1016/j.nucengdes.2017.12.016>.
- [40] J.D. Stempien, P.A. Demkowicz, J.M. Harp, P.L. Winston, AGR-3/4 Experiment Preliminary Mass Balance, Idaho National Laboratory, Idaho Falls, ID, 2018, p. 62.

- [41] J.M. Harp, P.A. Demkowicz, J.D. Stempien, Initial Gamma Spectrometry Examination of the AGR-3/4 Irradiation, 2016 International Topical Meeting on High Temperature Reactor Technology (HTR 2016), Las Vegas, NV, 2016.
- [42] X. Liu, X. Huang, F. Xie, F. Jia, X. Feng, H. Li, Source Term Analysis of the Irradiated Graphite in the Core of HTR-10, *Sci. Technol. Nucl. Install.* 2017 (2017) 1-6, <https://doi.org/10.1155/2017/2614890>.
- [43] M.A. Fütterer, L. Fu, C. Sink, S.d. Groot, M. Pouchon, Y.W. Kim, F. Carré, Y. Tachibana, Status of the very high temperature reactor system, *Prog. Nucl. Energy* 77 (2014) 266-281, <https://doi.org/10.1016/j.pnucene.2014.01.013>.
- [44] P.J. Pappano, T.D. Burchell, J.D. Hunn, M.P. Trammell, A novel approach to fabricating fuel compacts for the next generation nuclear plant (NGNP), *J. Nucl. Mater.* 381(1-2) (2008) 25-38, <https://doi.org/10.1016/j.jnucmat.2008.07.032>.
- [45] B.P. Collin, AGR-1 Irradiation Test Final As-Run Report, Idaho National Laboratory, Idaho Falls, ID, 2015, p. 99.
- [46] J.D. Hunn, M.P. Trammell, Data Compilation for AGC-2 Matrix-only Compact Lot A3-H08, Oak Ridge National Laboratory, Oak Ridge, TN, 2010, p. 39.
- [47] K. Verfondern, B. Liu, H. Nabelek, T. Wang, H.J. Allelein, C.H. Tang, Release Rates of Short-lived Fission Gases from Modern Spherical Fuel Elements with TRISO-coated Particles, *J. Phys.: Conf. Ser.* 2048 (2021) 1-12, [10.1088/1742-6596/2048/1/012010](https://doi.org/10.1088/1742-6596/2048/1/012010).
- [48] G.Q. Zheng, P. Xu, K. Sridharan, T.R. Allen, Pore Structure Analysis of Nuclear Graphites IG-110 and NBG-18, in: S.K. Sundaram, K. Fox, T. Ohji, E. Hoffman (Eds.), *Advances in Materials Science for Environmental and Nuclear Technology II*, Volume 227, The American Ceramic Society 2011, pp. 251-260.
- [49] HTGR Mechanistic Source Terms White Paper, Idaho National Laboratory, Idaho Falls, ID, 2010, p. 95.
- [50] B.P. Collin, Diffusivities of Ag, Cs, Sr, and Kr in TRISO Fuel Particles and Graphite, Idaho National Laboratory, Idaho Falls, ID, 2016, p. 40.
- [51] T.M. Weilert, K.L. Walton, S.K. Loyalka, J.D. Brockman, Measurement of effective Sr diffusion coefficients in IG-110 graphite, *J. Nucl. Mater.* 555 (2021), <https://doi.org/10.1016/j.jnucmat.2021.153102>.
- [52] Fuel performance and fission product behaviour in gas cooled reactors, International Atomic Energy Agency, Vienna, Austria, 1997, p. 529.
- [53] G.A. Cowan, C.J. Orth, Diffusion of fission products at high temperatures from refractory matrices, Second United Nations International Conference on the Peaceful Uses of Atomic Energy, U.S. Government Printing Office, 1958, p. 17.
- [54] C.J. Orth, Diffusion of Lanthanides and Actinides from Graphite at High Temperatures, *Nucl. Sci. Eng.* 9(4) (1961) 417-420, <https://doi.org/10.13182/NSE61-A25905>.
- [55] K. Hayashi, T. Kikuchi, F. Kobayashi, K. Minato, K. Fukuda, K. Ikawa, K. Iwamoto, Distribution of fission products in irradiated graphite materials of HTGR fuel assemblies: Third and fourth OGL-1 fuels, *J. Nucl. Mater.* 136(2-3) (1985) 207-217, [https://doi.org/10.1016/0022-3115\(85\)90008-X](https://doi.org/10.1016/0022-3115(85)90008-X).
- [56] K. Hayashi, F. Kobayashi, K. Minato, K. Ikawa, K. Fukuda, In-pile release behavior of metallic fission products in graphite materials of an HTGR fuel assembly, *J. Nucl. Mater.* 149(1) (1987) 57-68, [https://doi.org/10.1016/0022-3115\(87\)90498-3](https://doi.org/10.1016/0022-3115(87)90498-3).

- [57] B.F. Myers, D.D. Jensen, L.R. Zumwalt, The diffusion of cesium and strontium in H-327 graphite during the Peach Bottom Fuel Test Element experiments, in: E.H. (Ed.) (Ed.) Proceedings of a Colloquium held at Hahn-Meitner-Institut, Berlin, 1981, pp. 166-171.
- [58] L.M. Carter, J.D. Brockman, S.K. Loyalka, J.D. Robertson, Measurement of cesium diffusion coefficients in graphite IG-110, *J. Nucl. Mater.* 460 (2015) 30-36, <https://doi.org/10.1016/j.jnucmat.2015.01.055>.
- [59] L.M. Carter, J.D. Brockman, S.K. Loyalka, J.D. Robertson, Calibration of a system for measurements of diffusion coefficients of fission products in HTGR/VHTR core materials, *J. Radioanal. Nucl. Chem.* 307 (2016) 1771-1775, 10.1007/s10967-015-4633-0.
- [60] L.M. Carter, J.D. Brockman, J.D. Robertson, S.K. Loyalka, ICP-MS measurement of diffusion coefficients of Cs in NBG-18 graphite, *J. Nucl. Mater.* 466 (2015) 402-408, <http://dx.doi.org/10.1016/j.jnucmat.2015.08.023>.
- [61] L.M. Carter, J.D. Brockman, J.D. Robertson, S.K. Loyalka, ICP-MS measurement of iodine diffusion in IG-110 graphite for HTGR/VHTR, *J. Nucl. Mater.* 473 (2016) 218-222, <https://doi.org/10.1016/j.jnucmat.2016.03.001>.
- [62] L.M. Carter, J.D. Brockman, J.D. Robertson, S.K. Loyalka, Diffusion of cesium and iodine in compressed IG-110 graphite compacts, *J. Nucl. Mater.* 476 (2016) 30-35, <http://dx.doi.org/10.1016/j.jnucmat.2016.04.024>.
- [63] L.M. Carter, J.D. Seelig, J.D. Brockman, J.D. Robertson, S.K. Loyalka, ICP-MS measurement of silver diffusion coefficient in graphite IG-110 between 1048K and 1284K, *J. Nucl. Mater.* 498 (2018) 44-49, <https://doi.org/10.1016/j.jnucmat.2017.10.009>.
- [64] T.M. Weilert, K.L. Walton, S.K. Loyalka, J.D. Brockman, Effective diffusivity of Ag and migration of Pd in IG-110 graphite, *J. Nucl. Mater.* 559 (2022), <https://doi.org/10.1016/j.jnucmat.2021.153427>.
- [65] I.G. Hughes, T.P.A. Hase, Measurements and their Uncertainties: A Practical Guide to Modern Error Analysis, Oxford University Press 2010.
- [66] B.F. Myers, A review of the diffusion of selected fission product metals in polycrystalline graphite, in: E. Hoinkis (Ed.) Proceedings of a Colloquium held at Hahn-Meitner-Institut, Berlin, 1981, pp. 56-67.
- [67] B.F. Myers, W.E. Bell, Strontium transport data for HTGR systems, General Atomic Company, San Diego, CA, 1974, p. 75.
- [68] F.J. Sandalls, M.R. Walford, Laboratory determinations of strontium diffusion coefficients in graphite, *J. Nucl. Mater.* 62(2-3) (1976) 265-272, [https://doi.org/10.1016/0022-3115\(76\)90023-4](https://doi.org/10.1016/0022-3115(76)90023-4).
- [69] K.M. Adkison, S.-L. Shang, B.J. Bocklund, D. Klimm, D.G. Schlom, Z.-K. Liu, Suitability of binary oxides for molecular-beam epitaxy source materials: A comprehensive thermodynamic analysis, *APL Mater.* 8(8) (2020) 081110-1-18, <https://doi.org/10.1063/5.0013159>.